β-Technetium: An allotrope with a nonstandard volume-pressure relationship

Emily Siska,[1] Dean Smith,[2] Christian Childs,[3] Daniel Koury,[1] Paul M. Forster,[1] Keith V. Lawler,[1,*] and Ashkan Salamat[3,†]

[1]*Department of Chemistry & Biochemistry, University of Nevada Las Vegas, Las Vegas, Nevada 89154, USA*
[2]*HPCAT, X-ray Science Division, Argonne National Laboratory, Illinois 60439, USA*
[3]*Department of Physics & Astronomy, University of Nevada Las Vegas, Las Vegas, Nevada 89154, USA*

(Received 11 February 2021; revised 24 March 2021; accepted 4 May 2021; published 9 June 2021)

We report the synthesis and structure of the second allotrope of technetium, β-Tc. Transformative pathways are accessed at extreme conditions using the laser-heated diamond anvil cell and confirmed with *in situ* synchrotron x-ray diffraction and Raman spectroscopy. β-Tc is fully recoverable to ambient conditions, although counter to our DFT calculations predicting a face-centered-cubic lattice, we observe a tetragonal structure ($I4/mmm$) that exhibits further tetragonal distortion with pressure. β-Tc has an expanded volume relative to the hcp ground state phase, that when doped with nitrogen has an unexpected volume lowering. Such anomalous behavior is possibly indicative of a rare electronic phase transition in a 4d element.

DOI: 10.1103/PhysRevMaterials.5.063603

I. INTRODUCTION

Technetium's radioactivity and natural scarcity have led to limited experimental studies, especially at elevated pressures and temperatures. A more complete understanding of technetium would provide valuable insight to many other transition metals given its central position in the transition-metal block of the periodic table. Owing to the difficulty in working with technetium, its group-7 neighbor rhenium is often used as a stand-in [1]. Both technetium and rhenium have only one confirmed allotrope, an hcp metallic phase. Hcp Tc is known to be stable to the melt at ambient pressure and to 67 GPa at 300 K [2,3] while hcp Re is stable against 100 s of GPa of compression and predicted to be stable beyond the TPa regime [4,5]. In contrast, the other group-7 element manganese has five reported allotropes. Two of its polymorphs (α and β) have complicated crystal structures and α-Mn is a well-known antiferromagnet (AFM) [6–8]. Another polymorph, γ-Mn, is fcc in its 1368–1406 K stability window [9] but distorts into a bct phase below its Néel temperature due to its antiferromagntism [10,11]. When stabilized at ambient conditions, γ-Mn exhibits an expanded lattice – as much as a 10% increase in atomic volume is observed [12].

There have been reports of chemical synthesis and purification routes using either thin film grown epitaxially by ion sputtering or thermal decomposition involving Tc that have suggested a cubic (fcc) allotrope [13,14]. However, these results are treated with caution, as these studies have conflicting and unrepeatable results and their experimental procedures show that they are not within a single component composition. This is further evidenced by conflicting reports of elemental reactions between Tc and anion species, e.g., C, N, that all report similar unit cell parameters of approx. 3.98 Å—comparable to the unconfirmed reports of fcc Tc [2]. For Tc carbides, a recent publication refuted the existence of the experimentally reported high-temperature cubic phase of TcC based on evolutionary algorithm simulations [13]. It concludes that Tc_6C, the most stable carbide on the convex hull, could not be made, and that the cubic phase observed is a high-temperature cubic phase of elemental technetium which becomes thermodynamically stable above 1775 K. Such inconsistencies arise from elemental Tc not found naturally in the earth's crust and its purification being challenging.

In this paper, we unequivocally confirm the existence of the second allotrope of Tc that we designate as β-Tc. β-Tc is made at high-temperature, high-pressure conditions and is recoverable to ambient conditions without a substrate. X-ray diffraction (XRD), Raman spectroscopy, and scanning electron microscopy (SEM) measurements imply this is a pure allotrope of Tc with anomalous behavior not previously characterized. Room-temperature XRD reveals an expanded volume compared to the ground-state hcp phase and a tetragonal distortion while further compression reveals anomalous volume-pressure relations with a continuous deviation from an fcc motif. Density functional theory (DFT) simulations apt for a simple elemental metal are incongruent with the experimental results, indicating there is a complex underlying electronic behavior to this allotrope. We have synthesized β-Tc in two different chemical environments, Ar and N_2, and we note differences with their respective structural responses with pressure.

II. METHODS

Caution! ^{99}Tc is a weak β emitter (E_{max} = 293 KeV) with a half life of 200 000 years and no stable isotopes. Therefore, any manipulation of the material was performed in a posted radio-materials laboratory. All efforts followed locally approved handling and monitoring procedures for the specific radioisotope. Details on the containment of samples can be found in the Supplemental Material [15].

*keith.lawler@unlv.edu
†salamat@physics.unlv.edu

Hcp Tc metal samples were prepared by UNLV Radiochemistry following the route described in Silva emphet al. [16]. NH_4TcO_4, in a fused quartz boat, was placed in a tube furnace which was flushed with Ar at 300 °C and then ramped to 910 °C. This is followed by steam-reforming thermal reduction of TcO_2 at 910 °C under a wet Ar atmosphere in the presence of activated carbon. This method is shown to consistently produce pure Tc metal as characterized by transmission electron microscopy analysis, XRD, and electron energy loss spectrometry. Polycrystalline agglomerates of Tc metal were loaded into diamond anvil cells with diamonds ranging from 250–600 μm culets and gas loaded with either Ar or N_2 at 1.5 and 3 kbar, respectively. Double sided laser (Nd:YAG $\lambda = 1064$ nm) heating experiments were performed with *in situ* angle dispersive synchrotron XRD and optical pyrometry measurements at HPCAT, 16-ID-B of the Advanced Photon Source at Argonne National Laboratory ($\lambda = 0.406626$ Å). Significant consideration was given to ensure that the laser hot spot, focused x-ray beam, and the defined region of interest sampled by optical pyrometry were all spatially equivalent and aligned throughout the data acquisition [17]. Thermal radiation from the sample was collected and integrated by plotting light intensity as a function of wavelength and corrected for with a transfer function. Temperature measurements were determined by fitting the thermal emission spectra using Planck's distribution function for a black-body emitter, assuming a grey-body approximation. Pressure was determined with either the equation of state of Ar or ruby fluorescence [18,19]. SEM on the recovered sample was performed using a JEOL JSM-6700 field emission FE-SEM. In-house laser (YLF $\lambda = 1070$ nm) heating experiments were also performed using Raman scattering as a probe. Further details are in the Supplemental Material [15].

Plane-wave density functional theory [20,21] simulations were performed with the VIENNA AB INITIO SIMULATION PACKAGE version 5.4.4 using the generalized gradient approximation (GGA) functional of Perdew, Burke and Ernzerhof (PBE) [22]. The simulations used an evenly space Γ-centered k-point grid with 0.2 $Å^{-1}$ resolution [23]. As the system is metallic, the Brillouin zone was integrated with the first-order method of Methfessel and Paxton with a width of 0.20 eV [24]. The basis set cutoff energy was 600 eV using the projector augmented wave [25] pseudopotentials formulated for PBE (version 5.4) with valence configurations of $4p^6 5s^2 4d^5$ for Tc (i.e., "Tc_pv"), $2s^2 2p^3$ for N, and $2s^2 2p^2$ for C. Energy convergence tolerances for the self-consistent field steps were set to 10^{-9} eV and force convergence tolerances for the geometry optimizations to 10^{-4} eV $Å^{-1}$. To minimize the effect of Pulay stress, the volume-changing structural optimizations were performed in three parts: two sequential optimizations and a final single-point energy evaluation. Each optimization allowed all degrees of freedom to vary except for when a specific structural constraint was imposed as noted in the text, for instance, the c/a ratio along the Bain path.

III. RESULTS AND DISCUSSION

Hcp Tc was observed to be stable during laser heating from near ambient to pressures below 4 GPa and to temperatures up to and postquenching the melt. A typical XRD pattern of the hcp Tc starting material before laser heating is shown in Fig. 1. All peaks can be attributed to either hcp Tc or the inert Ar medium. While heating above 4 GPa at temperatures around 1500 K, hcp Tc was seen to transform to an allotrope, β-Tc. The transformation is marked by the appearance of a new set of Bragg peaks. β-Tc is fully recoverable to ambient conditions (XRD pattern and Rietveld fit of recovered sample in Supplemental Materials). Figure 1 contrasts the Le Bail refinements of the XRD patterns of hcp and β-Tc at 4.5 GPa and ambient temperature. Hcp Tc was fit with a previously determined $P6_3/mmc$ structure with starting values of $a = 2.7409$ Å and $c = 4.3987$ Å [26]. β-Tc can be indexed at this pressure by a tetragonal space group $I4/mmm$ with atoms on the $2a$ Wyckoff position, $a = 2.806(1)$ Å, and $c = 3.965(5)$ Å. This allotrope persists upon successive laser heating up to 2800 K at pressures between 10–30 GPa.

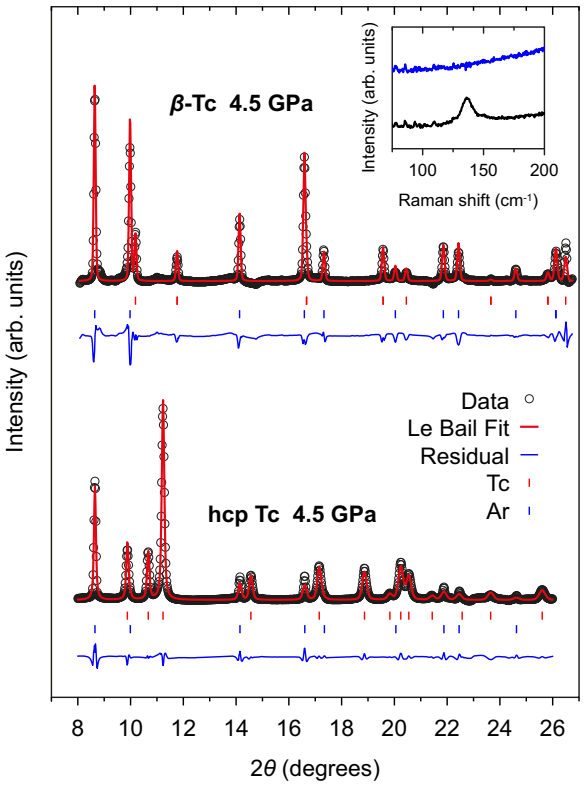

FIG. 1. XRD patterns of a Tc at room temperature pre (hcp, bottom) and post (β-Tc, top) laser heating. Black open circles are the experimental data, the Le Bail refinement is shown in red, and the residual is shown in blue. All peaks were attributed to Ar or Tc; tick marks for each phase shown below peaks. Inset: Raman spectrum of a room temperature Tc sample pre (hcp, black) and post (β-Tc, blue), laser heating.

The transformation into β-Tc can also be observed through Raman spectroscopy. The doubly degenerate E_{2g} phonon is the only Raman active optical mode of hcp Tc [27], observed here at 135 cm^{-1} at ambient conditions. The bct structure of β-Tc has a single atom primitive unit cell ergo no allowed optical Raman modes, leading to a featureless spectrum shown in the inset of Fig. 1. No evidence of other modes was observed across the full Raman spectral range, indicating that no other

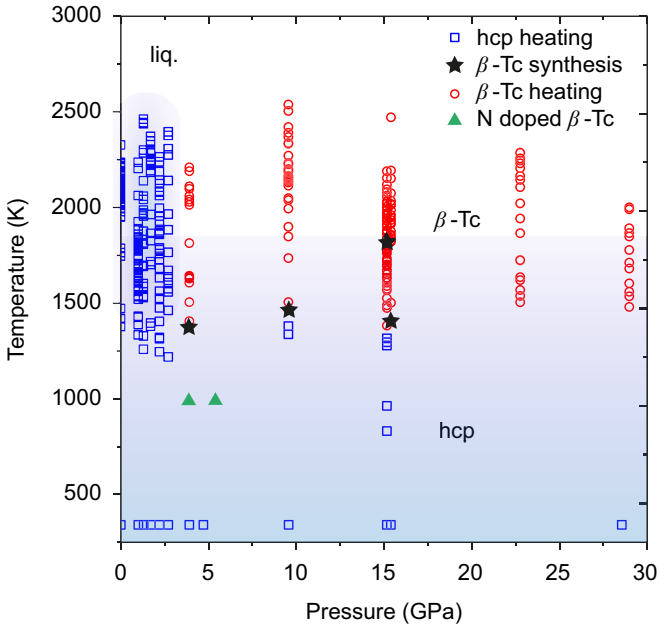

FIG. 2. Diagram showing the phase stability domains of hcp and β-Tc. The open markers represent a pressure-temperature condition where a single phase of hcp (squares) or bct (circles) could be confirmed by XRD. Stars indicate a point where the hcp-bct transformation was observed. Data at 15 GPa and 1800 K representing the transformation of β-Tc was uncharacteristically high due to a jump in temperature during laser heating, yet it is shown for completeness. Triangles indicate the P,T conditions where N-doped β-Tc is formed.

elements are present in significant enough concentration to provide a spectroscopic signature.

Using *in situ* XRD, the stability of the Tc allotropes were mapped as a function of both pressure and temperature, as summarized in Fig. 2. Below the critical transformation pressure of ~4 GPa, the hcp allotrope of Tc is stable—even after quenching from the melt. Above this critical pressure, the phase boundary is very steep and the transition temperature has no pressure dependence. The boundary was challenging to map above this pressure as the phase transformation process was observed to be sluggish. The data representative of β-Tc in Fig. 2 are shown only when a single phase was confirmed by XRD. The phase stabilities clearly demonstrate that the non-hcp allotrope can only be obtained through high temperatures coupled with high pressure.

The metastable recoverability to ambient conditions of the β-Tc phase is confirmed by XRD Rietveld analysis. Safety protocols do not allow for decompression of a radioactive sample during an experiment conducted at the APS, so all data was collected upon increasing pressure. Samples were decompressed and recovered once back at UNLV for further study. The Rietveld refinement of this recovered phase, however, showed some discrepancy between experimental and calculated peak intensities for the 112/200 and 103/211 peaks, yet the overall fit is very good with wRp = 9.4% and R = 4.5%. Surprisingly, the measured ambient volume of the new tetragonally indexed phase (15.92 Å^3/Tc, $a = 2.829(6)$ Å, $c = 3.99(1)$ Å) is significantly larger than the 14.31 Å^3/Tc volume of the hcp phase [3]. This volume difference is also

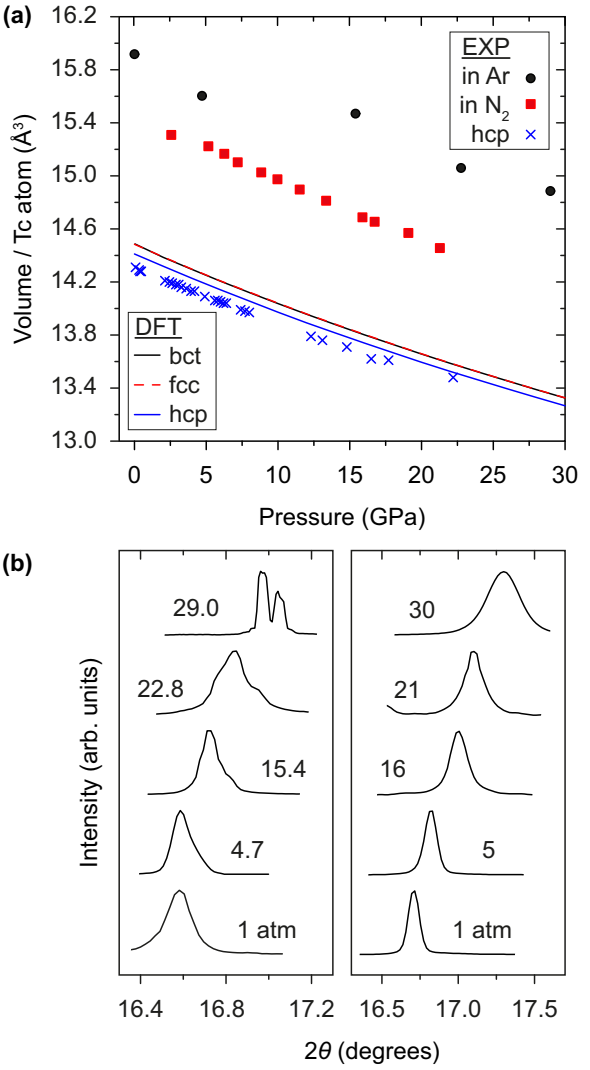

FIG. 3. (a) The difference in compression behavior of β-Tc at room temperature when formed in different PTM compared to simulations. Tabulated data points in Supplemental Material [15]; hcp experimental data is from Ref. [3]. (b) Left: Peak splitting of the 200 and 112 reflections as a function of pressure in β-Tc. Right: The absence of peak splitting in equivalent peaks of TcN_x.

large compared to previous shock simulations where the predicted fcc structure has an ambient volume much closer to that of the hcp phase, 14.501 Å^3/Tc [28].

The measured larger unit cell volume of the β-Tc phase compared to the ambient hcp phase is a fascinating observation that demands further thought [Fig. 3(a)]. A major chemical concern is whether the laser heating protocol is, in fact, leading to undesired Tc-carbide formation, leading to this observed volume expansion. To address this, we conducted these experiments 12 times, using laser heating methods over short timescales of 1–2 seconds to minimize any thermal buildup and the promotion of carbon diffusion from the diamond anvils. Our SEM and Raman spectroscopy measurements on recovered samples revealed no presence of carbide formation. Also, there is no known eutectic between Tc and C, and the most modern evolutionary algorithm simulations predict that Tc carbide is not energetically favorable. In the

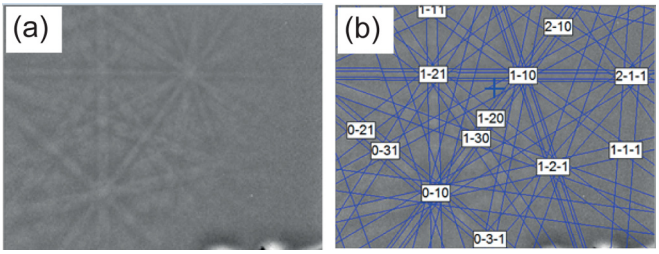

FIG. 4. EBSD results of the recovered Tc sample. (a) processed EBSD pattern and (b) indexed pattern as Tc phase with MAD = 0.6. The results of EBSD point analysis identifies an fcc lattice, and is consistent with the N-doped β-Tc phase as confirmed by Rietveld analysis using XRD.

TABLE I. A comparison of the DFT calculated properties for the experimentally determined bct β-Tc structures versus DFT relaxed hcp, bct, and fcc structures.

P (GPa)	Structure	a (Å)	c (Å)	c/a	Volume (Å^3/Tc)	Energy (meV/Tc)
0	hcp (DFT)	2.750	4.402	1.6007	14.41	0
	bct (expt)	2.829	3.990	1.4104	15.97	188
	bct (DFT)	2.738	3.864	1.4109	14.49	69
	fcc (DFT)	3.869	3.869	1.0000	14.48	69
4.5	hcp (DFT)	2.736	4.382	1.6012	14.11	0
	bct (expt)	2.806	3.965	1.4130	15.61	178
	bct (DFT)	2.723	3.851	1.4142	14.27	72
	fcc (DFT)	3.851	3.851	1.0000	14.27	72

case of Fe-C, it is important to note that the volume-carbon content relation for the bcc phase results in a volume lowering compared to the pure element [29].

Figure 3(a) plots experimental pressure/volume data of β-Tc synthesized in Ar and N_2 environments along with that of the hcp phase [3] and the DFT optimized hcp, fcc, and bct phases. Compression of β-Tc reveals that the tetragonal distortion present at ambient pressure becomes more pronounced with pressure. From 0–16 GPa, the tetragonal distortion hovers around $\Delta = 0.004$ ($c/a = 1.410$). Above 16 GPa, there is a sudden increase in the tetragonal distortion, becoming $\Delta = 0.013$ ($c/a = 1.401$) at 29 GPa. This is clearly observed in our XRD experiments through peak shifts that are inconsistent with a cubic structure and a peak splitting of the 200 and 211 peaks [Fig. 3(b), left panel] with compression. Critically, at the high temperatures where β-Tc is formed, the lattice is indexed as fcc and there is no observation of peak splitting observed at ambient temperature. It is not common for fcc-like metals to tetragonally distort with compression, nor has such a distortion been predicted for fcc Tc.

β-Tc was again synthesized, but in a N_2 media, in an effort to confirm whether a different chemical environment would permit the formation of this new phase, but at lower pressures. The critical condition to note here is that we observe no reaction between Tc and N_2 below a pressure of 4 GPa. This pure binary environment confirms that previous reports of Tc chemistry at ambient conditions are inconclusive. Above this critical pressure, the transformation temperature drops to approximately 1000 K. This difference in transition conditions is indicative of a chemical change in the system driven by the increased chemical potential of N_2 relative to Ar. β-Tc formed in N_2 is also recoverable to both ambient temperature and pressure. Energy-dispersive x-ray spectroscopy (EDX) measurements were performed on fully recovered doped β-Tc samples with a field emission SEM where point detection and mapping of the sample did not result any N detection (further details in Supplemental Material). The recovered sample of β-Tc formed in N_2 has an improved residual from crystallographic structure modeling with a cubic (fcc) structure rather than the bct structure formed in an Ar medium. Electron backscatter diffraction (EBSD) results confirm the recovered sample has an fcc lattice (Fig. 4). The cubic structure is maintained throughout the compression regime measured, with no evidence of a symmetry lowering or change [Fig. 3(b), right]. The samples made in N_2 also have smaller atomic volumes and a different compression response at room temperature to those made in Ar, as shown in Fig. 3(a). However, these volumes are still far too large (15.36 Å^3/Tc) to be consistent with our predicted fcc Tc structure described below (Table I). All these differences indicate β-Tc formed in N_2 is related but distinct from the synthesis in an Ar environment. Therefore, the formation in N_2 is most likely producing a doped version of β-Tc with interstitial nitrogen atoms.

DFT simulations on the experimentally determined bct ($I4/mmm$, $tI2$) structures for β-Tc at ambient and 4.5 GPa show it to be metastable versus the known hcp ground state at those pressures. Allowing the bct structures to relax improves their stability versus the hcp structure, however, they remain metastable but now with significantly reduced atomic volumes (see Table I). At ambient pressure, the optimized bct structure retains its tetragonal distortion, while at the elevated pressure it reverts to an fcc structure with $c/a = \sqrt{2}$. For comparison, the DFT optimized fcc structures are also displayed in Table I and they are consistent with those previously evaluated by DFT for an fcc Tc phase [13,28,30]. As a rudimentary structural survey provides no insight into the large atomic volume and tetragonal distortion observed for β-Tc, it is worth exploring the potential energy landscapes surrounding known transformations of an fcc metal. Along the Bain transformation path from bcc to fcc (in a $tI2$ representation) [31] in Fig. 5(a), there is only a single energetic minimum around the fcc structure which has a sigmoidal increase in energy toward the bcc structure ($c/a = 1$). This increase becomes steeper with pressure, explaining why the 4.5 GPa optimization of the experimental bct structure resorts to an fcc structure. There is little volume variance for the optimized structures along the Bain path, with the atomic volume capping at its largest value (14.6 Å^3/Tc at 0 GPa) for a c/a of 0.9. While the atomic volume is at its lowest around the fcc structure, it is simply too small anywhere along the Bain path (within the chosen electronic structure methodology) to explain what is observed experimentally for β-Tc synthesized in a noninteracting Ar environment.

As the Bain path indicates that no tetragonal modification of an fcc structure is favorable within the electronic structure method chosen, one can look to alternative modifications of the fcc structure to explain the experimental observations.

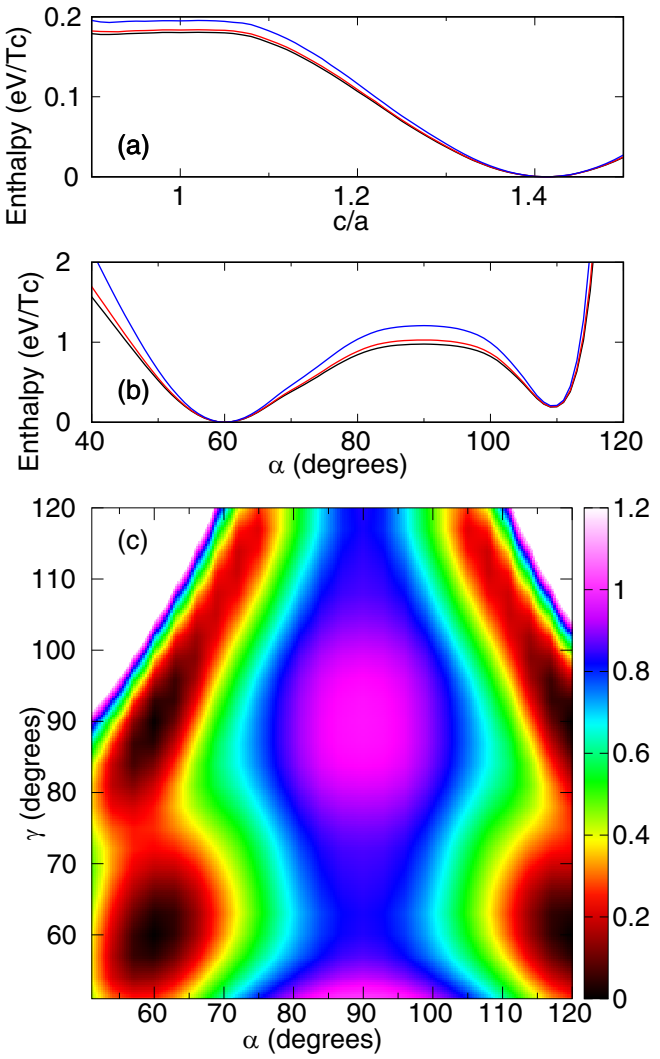

FIG. 5. (a) Enthalpy variation of the DFT optimized $tI2$ structures along the Bain path at 0 GPa (black), 5 GPa (red), and 25 GPa (blue). (b) Enthalpy variation of the DFT optimized $hR1$ structures with α at 0 GPa (black), 5 GPa (red), and 25 GPa (blue). (c) Heat map of the per atom enthalpy variation of a 0 GPa modified $hR1$ structure where $a = b = c$ but $\alpha = \beta \neq \gamma$. All enthalpies are relative to the fcc Tc structure, i.e., $c/a = \sqrt{2}$ for $tI2$ or $\alpha = \beta = \gamma = 60^\circ$ for $hR1$.

One alternative is distortions of the angles between the lattice vectors of the fcc $hR1$ primitive unit cell. Such rhombohedral distortions give rise to vanadium's bcc $\rightarrow$ $hR1$ $\rightarrow$ $hR1$ $\rightarrow$ bcc phase progression with pressure [32–34]. It should be noted that at lower pressures a tetragonal or rhombohedral modification of an fcc structure would be indistinguishable in the experimental XRD data, but over the full pressure range the tetragonally distorted structure is shown to be correct. Tracing the variation of the energy with respect to the rhombohedral angle of $hR1$ Tc [Fig. 5(b)] shows that once again the fcc structure ($\alpha = 60^\circ$) is the lowest energy structure at all pressures evaluated. The rhombohedral distortion landscape has a global minima about the fcc structure that increases to a local maximum around the simple cubic (sc) structure ($\alpha = 90^\circ$), evolving into a much sharper local minimum about the body-centered cubic structure ($\alpha = 109.47^\circ$). The only marked change to the relative energetics with pressure along this pathway is an increasing unfavorability of the sc structure; the relative stability of the bcc phase varies by only $\sim$1 meV/Tc GPa^{-1}. The atomic volumes are found to vary greatly with rhombohedral distortion between the bcc and fcc structures, where regardless of pressure the structures near $\alpha = 90^\circ$ become larger than those observed experimentally for β-Tc. They are also 9–12% larger than the predicted fcc/bcc structures.

The 0 GPa energy landscape in Fig. 5(c) expands on the analysis of a rhombohedral distortion by accounting for the one-atom primitive cell of the bct structure, taking on a lowered $hR1$-like symmetry with $a = b = c$ but $\alpha = \beta \neq \gamma$ ($\alpha \approx 119.9^\circ$ and $\gamma \approx 90.1^\circ$ for the experimental structures shown in Table I). The fcc structure appears at four points on the plotted landscape (α, γ: 60,60; 60,90; 120,60; and 120,90) and it is always the lowest energy structure regardless of pressure (5 GPa plot in the Supplemental Material). The Bain path as represented in Fig. 5(c) (between $\alpha = 120^\circ$, $\gamma = 90^\circ$ and $\alpha = \gamma = 109.47^\circ$) is the domain of greatest stability aside from the broad basin about the conventional $hR1$ fcc primitive unit cell, yet none of those structures thusly represented are stable or large enough to explain the experimental observations. Furthermore, the phonon band structure for fcc Tc at 0 and 5 GPa have no apparent Kohn anomolies (see Supplemental Material) which are attributed to vanadium's distorted phase progression [33,35,36]. Peierls instabilities have been attributed to symmetry-breaking distortions away from higher symmetry structures in known elemental systems like β-Sn, γ-Se, A17 P, and A7 P [37–41]. However, DFT optimizations of these structures for Tc either produced higher energies or resorted to the fcc structure itself, and attempts to refine the XRD data with these structures yielded worse fits of the data. Thus, within the weak electron correlation description of the GGA no common distortion is predicted to occur to explain the observations on β-Tc.

The previously discussed simulations continually produced structures with volumes too low compared to the experimental results, which is surprising as the PBE functional employed is well-known to typically overestimate the volume ($\leqslant 5\%$) of a system as may be seen in the comparison between the simulated and experimental volumes of the hcp phase in Fig. 3(a). On-atom electron localization through increased electron correlation effects is one possibility that could increase the atomic volumes, as it is known that with increased volume the individual atoms will tend towards a free-atom limit [42]. Screened on-site Coulomb interactions in the form of a Hubbard + U correction is one technique that can be used to correct an overly weak description of electron correlation in some density functionals and increase on-site localization of charge density [43]. We evaluated the ability of a single-parameter DFT + U applied to the Tc d electrons to determine if including such electron correlation effects could remedy the underprediction of the volumes by the conventional GGA [44,45]. The Hubbard parameter was determined using a linear response approach [46], giving $U_{eff} = 2.95$ eV for the ambient hcp phase of Tc and $U_{eff} = 3.15$ eV for the XRD determined ambient bct β-Tc structure, so a median value of $U_{eff} = 3.05$ eV was used in the simulations. As with the pure

GGA simulations, the GGA + U simulations underestimate the volume compared to the experimentally determined values with the predicted ambient fcc structure actually decreasing in volume by 0.03 $Å^3$/Tc in both the *tI*2 and *hR*1 representations. No new minima are observed with GGA + U along the Bain or rhombohedral transformation pathways. There is just a lowering of the energy penalty to adopt a non-fcc structure, i.e., both the bcc and sc phases became more stable by $\sim$ 0.08 eV/Tc in their 0 GPa *hR*1 representations. As every simulation run gave similar results whether or not a Hubbard correction was included, one can ascertain that slightly stronger electron correlations than described by PBE are alone not the cause for the curious properties observed for this Tc allotrope.

The effect of introducing varying amounts of nitrogen in the octahedral sites of an ambient pressure fcc Tc lattice was performed using DFT to determine if doping could explain what was observed for the synthesis of β-Tc in N_2. At the 3.5 wt % N level of doping, Tc_4N maintains a cubic structure with a volume beyond what was measured (16.1 $Å^3$/Tc). A step down in concentration to Tc_8N produces a 15.2 $Å^3$/Tc fcc Tc sublattice, close to what was measured experimentally and suggesting a dopant concentration of 1.8 wt % (11 atom %) N. However, the limits of detection for the EDX measurements are estimated to be slightly lower than this concentration (discussed in Supplemental Material). By a concentration below the estimated limit of detection, 0.5 wt % (3 at. %), the DFT optimized cell remains cubic but is only 14.7 $Å^3$/Tc, well below the measured value of the samples produced in N_2. While DFT does indicate that N doping can cause the structures observed for synthesizing β-Tc in N_2, the coarse agreement with experiment suggests that, like β-Tc formed in Ar, there is something more complicated occurring than can be predicted with a simple metallic picture.

Similar doping evaluations were done with carbon as the dopant, and in each case the carbon-doped cell is slightly larger than its nitrogen-doped counterpart. Carbon doping can be eliminated as a cause for the behavior observed for β-Tc synthesized in Ar as it would've required a concentration of nearly Tc_4C to obtain the volumes observed. A concentration that high is stoichiometric and should be detectable by XRD [13]; in addition, there is no detectable Raman signature that must arise from a solid with more than one element type in its primitive unit cell. Additionally, Ar is an inert PTM and highly unlikely to dope a sample in the same way, especially as it is very large compared to β-Tc with a 4.3 GPa, 300 K fcc lattice constant of 4.7 Å (i.e., an atomic volume of 25.98 $Å^3$) and a kinetic diameter of 3.542 Å [18,47].

In this light, β-Tc is best considered as a high-temperature phase of Tc. Although the shallow laser-heating skin depth doesn't allow for a reliable volume of hcp Tc at high temperature, our thermal (isobaric) volumetric trends seem to roughly follow those previously detailed [30,48]. Our most reliable high-temperature structural refinement of β-Tc in Ar (9.7 GPa, 2147 K) is fcc with a volume of 15.6 $Å^3$/Tc, whereas the hcp phase is roughly 15.0 $Å^3$/Tc at a similar temperature (0.1 GPa, 2263 K). Such an entropically favorable $\sim$ 5% increase in atomic volume is not unheard of for transitions into high-temperature phases. For instance, the atomic volume increases by 4% for the α-Mn to β-Mn transition at 1 atm [49] and 1–2% for ε-Fe to γ-Fe between 52 and 86 GPa [50]. Additionally, the prismatic hcp to fcc transition in Ti exhibits a 14.2–19.5% volume increase [51].

Furthermore, it is our hypothesis that β-Tc exhibits magnetic ordering, wherein the high-temperature fcc structure is paramagnetic (PM) and it tetragonally distorts into the bct structure as it crosses its Néel temperature somewhere above 300 K [42,52,53]. Preliminary DFT + U simulations support this hypothesis with AFM type-I ordering similar to γ-Mn (with spins antiparallel along the [001] easy axis) being the most energetically favorable magnetic/nonmagnetic configuration in the experimental bct structures and their similarly dimensioned fcc counterparts [10,11]. Likewise, the volume contraction of high-temperature β-Tc compared to ambient is likely analogous to Cr, which exhibits a volume contraction as it is heated through the first-order AFM to PM transition [54]. While an antiferromagnetic, high-temperature phase can explain many of the volume anomalies observed for β-Tc, further experimental developments are needed for confirmation.

IV. CONCLUSIONS

In conclusion, we have synthesized a metastable tetragonal allotrope of Tc using high-temperature and high-pressure conditions that is fully recoverable to ambient conditions. β-Tc tetragonally distorts at room temperature, evident from the splitting of the 200 and 211 XRD peaks. The tetragonal distortion becomes more pronounced with increased pressure indicating a pressure-volume response quite dissimilar to what should be expected for a conventional fcc elemental phase, in particular for a 4*d* transition metal whose behavior could be anticipated to be nearly free electronlike. DFT simulations using the GGA are unable to fully explain the behavior observed for this allotrope, further confirming that the phase is more complicated than a conventional fcc metal. The behavior of β-Tc has likely been previously overlooked because of this nonstandard behavior and we are working toward a concrete theoretical and experimental identification of the cause of this behavior. Samples of β-Tc synthesized in N_2 instead of Ar have a slightly different behavior, remaining cubic when quenched to ambient. The volumetric response and DFT simulations indicate the samples produced in N_2 are β-Tc doped to a concentration upward of Tc_8N, although a deeper understanding of the anomalous behavior of the samples produced in Ar will likely change this value. We suspect that previously reported but hard to replicate compounds like TcC or $TcN_{0.75}$ are likely β-Tc stabilized by impurities such as carbon, oxygen, or nitrogen [13,55,56].

ACKNOWLEDGMENTS

The authors thank Curtis Kenney-Benson for technical development. This material is based upon work supported by the National Science Foundation Division of Materials Research under Grant No. 1904694. Portions of this work were performed at HPCAT (Sector 16), Advanced Photon Source (APS), Argonne National Laboratory. HPCAT operations are supported by DOE-NNSA Office of Experimental Sciences. Other portions of this work were performed at GeoSoilEnviroCARS (University of Chicago, Sector 13), Advanced Photon Source (APS), Argonne National Laboratory.

GeoSoilEnviroCARS is supported by the National Science Foundation—Earth Sciences (EAR No. 1634415) and Department of Energy—GeoSciences (DE-FG02-94ER14466). The APS is a U.S. Department of Energy (DOE) Office of Science User Facility operated for the DOE Office of Science by Argonne National Laboratory under Contract No. DE-AC02-06CH11357. Computational resources were provided by the UNLV National Supercomputing Institute.

[1] N. N. Greenwood and A. Earnshaw, *Chemistry of the Elements*, 2nd ed. (Reed Educational and Professional Publishing Ltd., Oxford, 1997).
[2] K. Schwochau, *Technetium* (Wiley-VCH, Weinheim, 2000).
[3] D. S. Mast, E. Kim, E. M. Siska, F. Poineau, K. R. Czerwinski, B. Lavina, and P. M. Forster, J. Phys. Chem. Solids **95**, 6 (2016).
[4] L. Dubrovinsky, N. Dubrovinskaia, V. B. Prakapenka, and A. M. Abakumov, Nat. Commun. **3**, 1163 (2012).
[5] G. L. Rech, J. E. Zorzi, and C. A. Perottoni, Phys. Rev. B **100**, 174107 (2019).
[6] J. S. Kasper and B. W. Roberts, Phys. Rev. **101**, 537 (1956).
[7] J. A. Oberteuffer, J. A. Marcus, L. H. Schwartz, and G. P. Felcher, Phys. Rev. B **2**, 670 (1970).
[8] A. C. Lawson, A. C. Larson, M. C. Aronson, S. Johnson, Z. Fisk, P. C. Canfield, J. D. Thompson, and R. B. Von Dreele, J. Appl. Phys. **76**, 7049 (1994).
[9] *3d, 4d and 5d Elements, Alloys and Compounds*, Landolt-Börnstein—Group III Condensed Matter, edited by H. Wijn Vol. 19a (Springer-Verlag, Berlin, 1986).
[10] T. Oguchi and A. Freeman, J. Magn. Magn. Mater. **46**, L1 (1984).
[11] H. Duschanek, P. Mohn, and K. Schwarz, Phys. B: Condens. Matter **161**, 139 (1990).
[12] I. Di Marco, J. Minár, J. Braun, M. I. Katsnelson, A. Grechnev, H. Ebert, A. I. Lichtenstein, and O. Eriksson, Eur. Phys. J. B **72**, 473 (2009).
[13] Q. Wang, K. E. German, A. R. Oganov, H. Dong, O. D. Feya, Y. V. Zubavichus, and V. Y. Murzin, RSC Adv. **6**, 16197 (2016).
[14] I. V. Vinogradov, M. I. Konarev, L. L. Zajtseva, and S. V. Shepel'kov, Zhurnal Neorganicheskoj Khimii **23**, 639 (1978).
[15] See Supplemental Material at http://link.aps.org/supplemental/10.1103/PhysRevMaterials.5.063603 for additional experimental methodology including radiation containment and temperature measurements, XRD data, and simulation data.
[16] G. W. C. Silva, F. Poineau, L. Ma, and K. R. Czerwinski, Inorg. Chem. **47**, 11738 (2008).
[17] S. Petitgirard, A. Salamat, P. Beck, G. Weck, and P. Bouvier, J. Synchrotron Radiat. **21**, 89 (2014).
[18] H. Marquardt, S. Speziale, A. Gleason, S. Sinogeikin, I. Kantor, and V. B. Prakapenka, J. Appl. Phys. **114**, 093517 (2013).
[19] A. Dewaele, P. Loubeyre, and M. Mezouar, Phys. Rev. B: Condens. Matter Mater. Phys. **70**, 094112 (2004).
[20] P. Hohenberg and W. Kohn, Phys. Rev. **136**, B864 (1964).
[21] W. Kohn and L. J. Sham, Phys. Rev. **140**, A1133 (1965).
[22] J. P. Perdew, K. Burke, and M. Ernzerhof, Phys. Rev. Lett. **77**, 3865 (1996).
[23] J. D. Pack and H. J. Monkhorst, Phys. Rev. B **16**, 1748 (1977).
[24] M. Methfessel and A. T. Paxton, Phys. Rev. B **40**, 3616 (1989).
[25] P. E. Blöchl, Phys. Rev. B **50**, 17953 (1994).
[26] J. A. Rard, M. H. Rand, G. Andregg, and H. Wanner, *Chemical Thermodynamics of Technetium*, Chemical Thermodynamics, edited by M. C. A. Sandino and E. Oesthols, Vol. 3 (OECD Nuclear Energy Agency, Data Bank, 1999).
[27] E. Kroumova, M. I. Aroyo, J. M. Perez-Mato, A. Kirov, C. Capillas, S. Ivantchev, and H. Wondratschek, Phase Transit. **76**, 155 (2003).
[28] E. Kim, P. F. Weck, and T. R. Mattsson, J. Appl. Phys. **124**, 035903 (2018).
[29] J. Yang, Y. Fei, X. Hu, E. Greenberg, and V. B. Prakapenka, Minerals **9**, 720 (2019).
[30] P. F. Weck and E. Kim, Dalton Trans. **44**, 12735 (2015).
[31] E. C. Bain, Trans. Am. Inst. Min. Metall. Eng. **70**, 25 (1924).
[32] Y. Ding, R. Ahuja, J. Shu, P. Chow, W. Luo, and H.-k. Mao, Phys. Rev. Lett. **98**, 085502 (2007).
[33] W. Luo, R. Ahuja, Y. Ding, and H.-k. Mao, Proc. Natl. Acad. Sci. **104**, 16428 (2007).
[34] A. K. Verma and P. Modak, Europhys. Lett. **81**, 37003 (2007).
[35] B. Grabowski, T. Hickel, and J. Neugebauer, Phys. Rev. B **76**, 024309 (2007).
[36] P. Souvatzis and O. Eriksson, Phys. Rev. B **77**, 024110 (2008).
[37] R. Keller, W. B. Holzapfel, and H. Schulz, Phys. Rev. B **16**, 4404 (1977).
[38] A. Decker, G. A. Landrum, and R. Dronskowski, Z. Anorg. Allg. Chem. **628**, 295 (2002).
[39] J.-P. Gaspard, C. R. Phys. **17**, 389 (2016).
[40] L. A. Falkovsky, JETP Lett. **103**, 106 (2016).
[41] D. Scelta, A. Baldassarre, M. Serrano-Ruiz, K. Dziubek, A. B. Cairns, M. Peruzzini, R. Bini, and M. Ceppatelli, Angew. Chem. Int. Ed. **56**, 14135 (2017).
[42] V. L. Moruzzi and P. M. Marcus, Phys. Rev. B **42**, 10322 (1990).
[43] A. I. Liechtenstein, V. I. Anisimov, and J. Zaanen, Phys. Rev. B **52**, R5467 (1995).
[44] S. L. Dudarev, G. A. Botton, S. Y. Savrasov, C. J. Humphreys, and A. P. Sutton, Phys. Rev. B **57**, 1505 (1998).
[45] M. K. Horton, J. H. Montoya, M. Liu, and K. A. Persson, npj Comput. Mater. **5**, 64 (2019).
[46] M. Cococcioni and S. de Gironcoli, Phys. Rev. B **71**, 035105 (2005).
[47] J.-R. Li, R. J. Kuppler, and H.-C. Zhou, Chem. Soc. Rev. **38**, 1477 (2009).
[48] Y. Shirasu and K. Minato, J. Alloys Compd. **335**, 224 (2002).
[49] N. Schmitz-Pranghe and P. Duenner, Z. Metallkd. **59**, 377 (1968).
[50] S. Anzellini, A. Dewaele, M. Mezouar, P. Loubeyre, and G. Morard, Science **340**, 464 (2013).
[51] J. X. Yang, H. L. Zhao, H. R. Gong, M. Song, and Q. Q. Ren, Sci. Rep. **8**, 1992 (2018).
[52] P. Schieffer, C. Krembel, M. Hanf, D. Bolmont, and G. Gewinner, J. Magn. Magn. Mater. **165**, 180 (1997).
[53] B. Schirmer, B. Feldmann, A. Sokoll, Y. Gauthier, and M. Wuttig, Phys. Rev. B **60**, 5895 (1999).
[54] A. Kaiser, J. Magn. Magn. Mater. **43**, 213 (1984).
[55] W. Trzebiatowski and J. Rudziński, Z. Chem. **2**, 158 (1962).
[56] W. Trzebiatowski and J. Rudzinski, J. Less-Common Met. **6**, 244 (1964).